NANO LETTERS

Letter

pubs.acs.org/NanoLett

High-Speed AFM Images of Thermal Motion Provide Stiffness Map of Interfacial Membrane Protein Moieties

Johannes Preiner,*[,†,‡] Andreas Horner,[‡] Andreas Karner,[†] Nicole Ollinger,[‡] Christine Siligan,[‡] Peter Pohl,[‡] and Peter Hinterdorfer[†,‡]

[†]Center for Advanced Bioanalysis GmbH, Gruberstrasse 40, 4020 Linz, Austria

[‡]Institute of Biophysics, Johannes Kepler University Linz, Gruberstrasse 40, 4020 Linz, Austria

Supporting Information

ABSTRACT: The flexibilities of extracellular loops determine ligand binding and activation of membrane receptors. Arising from fluctuations in inter- and intraproteinaceous interactions, flexibility manifests in thermal motion. Here we demonstrate that quantitative flexibility values can be extracted from directly imaging the thermal motion of membrane protein moieties using high-speed atomic force microscopy (HS-AFM). Stiffness maps of the main periplasmic loops of single reconstituted water channels (AqpZ, GlpF) revealed the spatial and temporal organization of loop-stabilizing intraproteinaceous H-bonds and salt bridges.

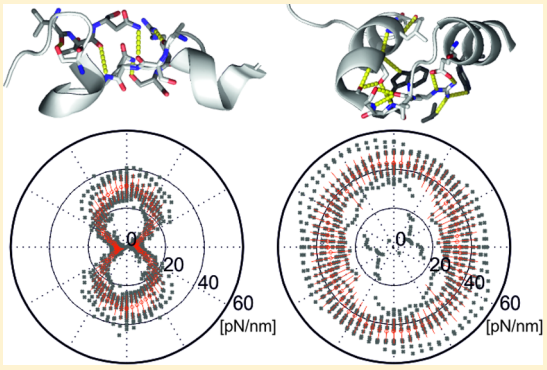

KEYWORDS: *Single molecule, flexibility, high speed atomic force microscopy, AqpZ, GlpF, membrane proteins*

Membrane proteins represent one of the main pharmaceutical targets. Yet docking studies are fraught with the difficulties of predicting the flexibility of extracellular loops. Studies of cell signaling face the same problem: highly variable extracellular loops govern ligand binding and activation mechanism of G-protein-coupled receptors.[1] Accurate predictions are difficult to compile, as small changes in amino acid position and orientation relative to both the membrane surface and to neighboring moieties may significantly alter the interaction forces with other loops and, therefore, its flexibility. For example, the bridge energy between oppositely charged amino acids may well be determined in aqueous solution,[2] but due to large contributions of the desolvation energies of the binding partners and interactions with other parts of the protein the total energy of salt bridges is difficult to estimate.[3] The situation is even more complicated in the case of interfacial membrane protein loops, because the desolvation energy depends on the dielectric permittivity ε that rapidly increases from 2 inside the membrane to 80 in the bulk. ε is likely to be around 10−20 immediately adjacent to the membrane surface,[4] but depending on the exact position of the loop ε may adopt any value between ∼4 and 40.[5] Likewise, the uncertainties in both ε and orientation render energy assessments impossible for (i) induced dipole−induced dipole interactions that make a significant contribution to van der Waals forces and (ii) for hydrogen bonds as their force is determined by the distance dependence of charge-dipole interactions.

Substitution of theoretical approaches for experimental means is also not straightforward. Classical methods like NMR, X-ray diffraction, and neutron scattering determine flexibilities from either thermal fluctuations on picosecond time scales[6] or disorder in protein conformations (B-factors). These techniques do not provide quantitative flexibility values of individual protein subdomains.[7] Advances in atomic force microscopy (AFM) imaging have yielded the average elasticity of membrane proteins[8] and, more recently, imaging modes based on indentation force spectroscopy[9] and force volume measurements[10,11] allowed for mapping the flexibility of α-helices and interhelical loops embedded in two-dimensional protein arrays in terms of resistance to vertical forces. In complementary approaches based on high-resolution AFM topographs of two-dimensional membrane protein crystals,[12,13] the energy landscape underlying the lateral thermal motion of polypeptide loops was reconstructed from the variability of protein topographies in the ensemble. As conventional AFM can only show static or slow time-lapse images of proteins, this analysis was restricted to proteins immobilized in two-dimensional crystals. The evolution of high speed AFM (HS-AFM) has led to instruments that overcome these limitations, enabling to follow the motion of single proteins[14−18] with subsecond temporal and subnanometer spatial resolution. This avoids ensemble averaging and therefore yields submolecular information on dynamics. In this study, we directly assessed the topographical variability of individual protein subdomains on a

Received: November 21, 2014
Revised: December 11, 2014

   dx.doi.org/10.1021/nl504478f | *Nano Lett.* XXXX, XXX, XXX−XXX

subsecond time scale to (I) deduce the energy landscape underlying subdomain motion, and (II) to derive quantitative stiffness values of the corresponding protein moieties by approximating the local energy landscape using a simple harmonic potential. As a model system, we have chosen two structurally highly homologous aquaporins (AQPs) from *E. coli*, the orthodox water channel AqpZ and the glycerol uptake facilitator GlpF.[19] Both proteins are homotetramers of four water/glycerol conducting channels, each of which consists of six transmembrane helices and two half-spanning helices joined end-to-end in the middle of the membrane. Comparison of the two structures[20,21] (Figure 1a) revealed an extremely high

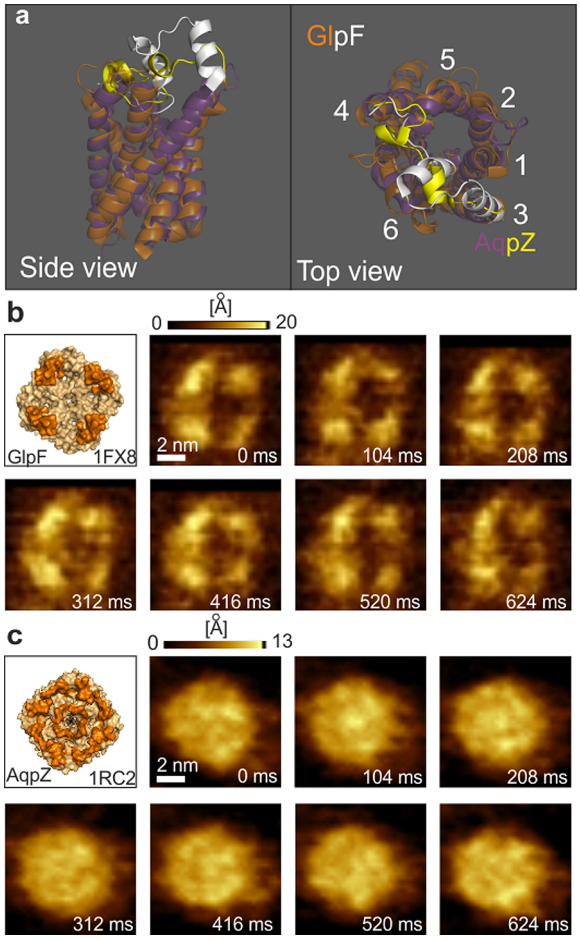

Figure 1. Structural homology and high speed AFM imaging of Glpf and AqpZ. (a) Structural alignment of GlpF (PDB 1FX8,[20] orange) and AqpZ (PDB 1RC2,[21] purple). The periplasmic loops are colored in white (GlpF) and yellow (AqpZ). Alignment was done using PyMol.[28] (b) GlpF surface representation with the membrane protruding periplasmic loops colored in orange and HS-AFM time series of a single GlpF tetramer embedded in a supported lipid bilayer. (c) AqpZ surface representation with the membrane protruding periplasmic loops colored in orange and HS-AFM time series of a single AqpZ tetramer embedded in a supported lipid bilayer.

degree of homology with the major structural difference located at the periplasmic side: The loop connecting transmembrane helices 3 and 4 (from now on called loop C) is significantly shorter and without distinct secondary structural elements (except two small helix turns) in AqpZ (yellow), whereas in GlpF (white) the loop contains 12 additional amino acids collectively possessing a more pronounced secondary structure. As the loops' spanning distance as well as the other structural elements are vastly identical, the flexibility of the loops is proposed to be mainly determined by their structure and its inter- and intramolecular interactions with its local environment.

Supported lipid bilayers were generated on freshly cleaved mica by fusion of proteoliposomes containing either GlpF or AqpZ. The proteins were functionally active as they increased the rate of water efflux from osmotically challenged vesicles in a stopped flow assay.[22] High-resolution imaging of individual GlpF tetramers embedded in the lipid bilayer (Supporting Information Movie S1; image sequence Figure 1b) revealed the periplasmic surface (cf. Supporting Information Figure S2) featuring four prominent protrusions with heights of 1.58 ± 0.28 nm (average topograph calculated from Supporting Information Movie S1, Figure 2a), resembling the membrane

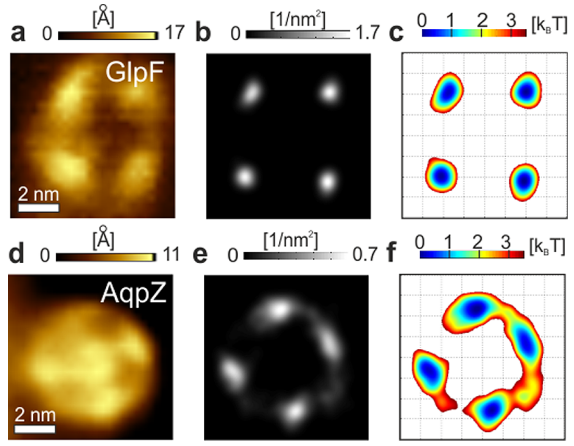

Figure 2. Configuration space and energy landscape underlying loop motions. (a) Average GlpF topography obtained from a time series (n = 37) of subsequent HS-AFM images. (b) Position probability map of GlpFs main periplasmic loop. (c) Energy landscape underlying the thermal motion of GlpFs main periplasmic loop calculated from the position probability map (b) by eq 2. (d) Average AqpZ topography generated from a time series (n = 85) of subsequent HS-AFM images. (e) Position probability map of AqpZs main periplasmic loop. (f) Energy landscape underlying the thermal motion of AqpZs main periplasmic loop calculated from the position probability map (e) by eq 2.

protruding loops known from crystal structure (cartoon representation (white) Figure 1a; surface representation (orange) Figure 1b). After the HS-AFM movie was corrected for collective motion (instrumental drift and slight diffusion) of the whole tetramer, (i.e., the coordinate system was transferred into the center of mass of the tetramer, cf. methods), the remaining loop motions reflected random thermal movement.[12] High-resolution topographs of individual AqpZ embedded in a supported lipid bilayer were recorded with comparable submolecular resolution, revealing details of AqpZ's periplasmic surface (Supporting Information Movie S2; image sequence Figure 1c; Supporting Information Figure S1). In accordance with the crystal structures (cartoon representation (yellow) Figure 1a; surface representation (orange) Figure 1c), the height of the protrusions are significantly lower (0.93 ± 0.17 nm, average topograph calculated from Supporting Information Movie S1, Figure 2a) compared to GlpF. Slightly smaller height values have been reported for these periplasmic surface protrusions under different experimental conditions from

dx.doi.org/10.1021/nl504478f | *Nano Lett.* XXXX, XXX, XXX−XXX

AqpZ 2D crystals embedded in DMPC/POPC (1:1) lipid bilayer.[13,23] Again, the variability of AqpZ from one topograph to the other (Supporting Information Movie S2) reflects thermal movement of the corresponding loops. As the thermal motion of the respective loop probes its configuration space over time, the free energy surface underlying the loop motion can be extracted from the probability distribution of loop positions[12] that were collected from the image sequences and are shown in Figure 2b,e, respectively. In the canonical ensemble, the probability distribution of loop positions $p(x,y)$ and the potential well $E(x,y)$ in which the particular loop is trapped are related by the equation

$$p(x, y) = C \exp\left(\frac{-E(x, y)}{k_B T}\right) \quad (1)$$

and the local free energy landscape can be estimated by

$$E(x, y) = C' - k_B T \ln(p(x, y)) \quad (2)$$

C' represents the Helmholtz free energy that is constant for a particular loop. Application of eq 2 to the probability distributions (Figure 2b,e) yields the free energy landscape underlying the motions of GlpFs (Figure 2c) and AqpZs (Figure 2f) loop C. The energy landscape of AqpZs loop C resembles a tangentially (with respect to the center of the tetramer) elongated groove, and the overall shape deduced here from time averaging of individual AqpZ embedded in their native lipid environment closely resembles the energy landscape of AqpZ deduced from ensemble averaging.[12] However, a closer inspection of the energy landscape reveals slight morphological differences among the four monomers making up the tetramer that most likely reflect different configurations of the respective loops. GlpFs loop C is trapped in a more confined, less asymmetric potential well. To quantify the stiffness k of the loops parallel to the membrane plane, we took radial cross sections through the potential wells and fitted them with a harmonic potential according to

$$E(r) = \frac{k}{2} r^2 \quad (3)$$

Supporting Information Figure S3 exemplifies such cross sections (black solid lines) and corresponding fits (red dashed lines) taken radially through the center of the GlpF (Supporting Information Figure S3a) and AqpZ (Supporting Information Figure S3b) tetramers. In this way, we have mapped the lateral stiffness values of the individual loops as a function of direction (angular increment 5°) onto the structures in Figure 3a (GlpF) and Figure 3c (AqpZ). Loop C in GlpF is the extension of an α-helix which is linked to its intramembrane part by a glycine residue. Because this glycine acts like a hinge, the lateral stiffness of the loop is mainly determined by the interaction with neighboring moieties. This is also true for the α-helical part of loop C from AQPZ, because it is enclosed between two short segments that appear unstructured in the crystal structure. Beside gradual stiffness variability among individual loops, the lateral stiffness maps (Figure 3a,c), reveal that the overall dependence on the direction is clearly different between GlpF and AqpZ, as can be seen from the ensemble plots of lateral stiffness values, Figure 3b,d. In the case of GlpF (Figure 3b), loop C exhibits a lateral stiffness that is only slightly dependent on the direction within the x–y plane (k_{max} = 43.6 ± 5.8 pN/nm; k_{min}= 32.8 ± 9.9 pN/nm; mean ± s.d.; n = 12), whereas the angular dependence of

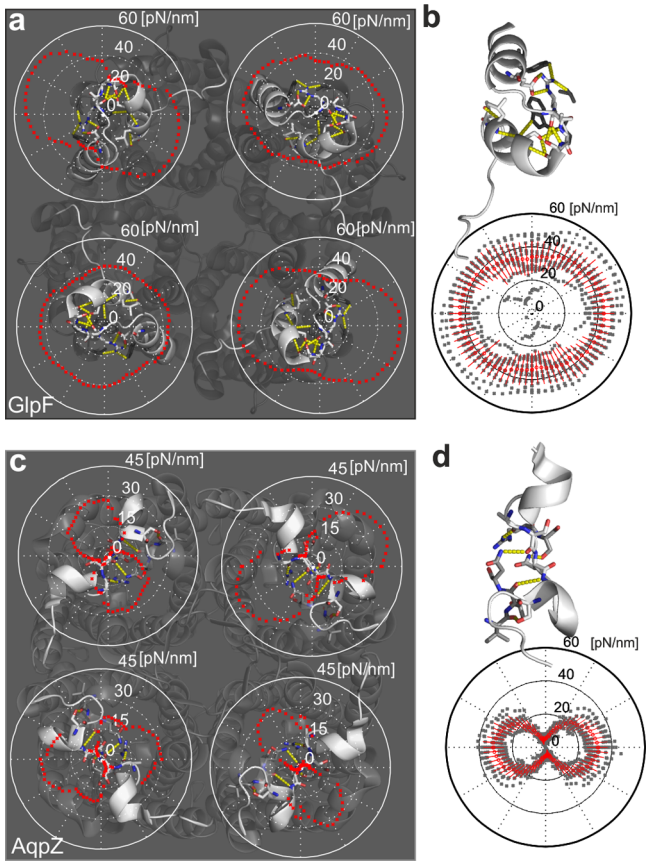

Figure 3. Mapping the stiffness values on GlpF and AqpZ. (a) Lateral stiffness (polar coordinates) of GlpFs loop C deduced from the energy landscape (Figure 2c) and overlaid on the GlpF X-ray structure. (b) Top: Crystal structure of GlpFs loop C. Stabilizing H-bonds and salt bridges as suggested from PyMol[28] are displayed as yellow dashed lines. Residues contributing to salt bridges and H-bonds are shown as sticks. Bottom: Ensemble plot (gray) and mean ± s.d. (red) of lateral stiffness values (polar coordinates; rotationally aligned to the crystal structure, top) deduced from 12 individual GlpF monomers taken from 3 individual GlpF tetramers (each taken from a different protein-reconstitution). (c) Lateral stiffness (polar coordinates) of AqpZs loop C deduced from the energy landscape (Figure 2f) and overlaid on the AqpZ X-ray structure. (d) Top: Crystal structure of AqpZs loop C. Stabilizing H-bonds and salt bridges as suggested from PyMol[28] are displayed as yellow dashed lines. Residues contributing to salt bridges and H-bonds are shown as sticks. Bottom: Ensemble plot (gray) and mean ± s.d. (red) of lateral stiffness values (polar coordinates; rotationally aligned to the crystal structure, top) deduced from 12 individual AqpZ monomers taken from 3 individual AqpZ tetramers-(each taken from a different protein-reconstitution).

AqpZs loop C lateral stiffness is highly asymmetric, being less stiff in the direction connecting helices 3 and 4 compared to the perpendicular direction (Figure 3d; k_{max} = 31.9 ± 4.5 pN/nm; k_{min} = 4.8 ± 1.9 pN/nm; mean ± s.d.; n = 12). Remarkably, in both cases the angular dependence of loop stiffness correlates with the direction and the amount of potential salt bridges and H-bonds connecting the respective loop to other structural elements of GlpF and AqpZ; The GlpFs bonds (n = 13; yellow lines, Figure 3b top; Supporting Information Figure S4a) are almost uniformly distributed among the directions in the x–y plane whereas AqpZs bonds (n = 5) are mainly aligned perpendicular to the direction connecting helices 3 and 4 (yellow lines, Figure 3d; Supporting Information Figure S4b).

dx.doi.org/10.1021/nl504478f | Nano Lett. XXXX, XXX, XXX–XXX

We conclude that high-speed AFM has the potential to quantitatively assess the flexibility of protein moieties on the surface of individual membrane proteins on a subsecond time scale without ensemble averaging simply by imaging and evaluating their thermal motion. This information should prove to be invaluable for the improvement of in silico docking studies. Matching the flexibility map with the network of polar bonds from structural models offers the possibility to validate results that were obtained under nonphysiological conditions, as with X-ray crystallography or electron microscopy. The flexibility map may also ease the prediction of the conformational transitions that membrane transporters and channels undergo when interacting with their substrate.

Methods. *HS-AFM Apparatus and Cantilevers.* High-speed AFM[14] was operated in tapping mode at room temperature (25 °C) with free amplitudes of 1.5−2.5 nm and an amplitude set point of larger than 90%. Silicon nitride cantilevers, (BL-AC10DS-A2, Olympus, Tokyo, Japan) with nominal spring constants of 0.1 N/m, a resonance frequency of ∼500 kHz, and a quality factor of ∼2 in liquids were used.

Image Analysis. Images were analyzed in ImageJ (NIH). Images were corrected for slight diffusion/drift of the tetramers via a slice alignment plugin.[24] The position of loops in each image frame was determined using a plug-in for multiple particle detection and tracking (ParticleTracker v. 1.5[25]), similar as described.[13] Loop positions were further processed using in-house algorithms implemented in MATLAB (MathWorks).

Sample Preparation. GlpF and AQPZ were expressed, purified, and reconstituted into *E. coli* total lipid extract (Avanti Polar Lipids, Alabaster, AL, U.S.A.) as previously described.[26,27] Proteoliposomes were extruded through two stacked 100 nm polycarbonate filters (Avestin, Ottawa, Canada). The reconstituted aquaporins were subjected to a functional test in a stopped flow apparatus. Their single channel water permeability was derived as previously described.[22] Functional proteoliposome samples were diluted 10-fold in measurement buffer (20 mM HEPES, 100 mM NaCl, pH 7.4) to a concentration of 1 mg/mL. A 2 μL droplet of this solution was applied to freshly cleaved mica for 10−15 min followed by rinsing and subsequent imaging in measurement buffer.

■ ASSOCIATED CONTENT

Ⓢ Supporting Information

Orientation of AqpZ in supported lipid membranes (Figure S1), orientation of GlpF in supported lipid membranes (Figure S2), determination of the loop stiffness (Figure S3), Polar contacts stabilizing Glpf and AqpZ loop C as suggested from crystal structure (Figure S4), High speed AFM movie of GlpF (Movie S1), and High speed AFM movie of AqpZ (Movie S2). This material is available free of charge via the Internet at http://pubs.acs.org.

■ AUTHOR INFORMATION

Corresponding Author

*E-mail: Johannes.Preiner@cbl.at.

Author Contributions

The manuscript was written through contributions of all authors. All authors have given approval to the final version of the manuscript.

P.P. and P.H. contributed equally.

Funding

This work was supported by the European Fund for Regional Development (EFRE, Regio 13), the Federal State of Upper Austria and the Austrian Science Foundation (FWF, P23466 to P.P. and P25844 to J.P.).

Notes

The authors declare no competing financial interest.

■ ACKNOWLEDGMENTS

We thank C. Rankl for fruitful discussions.

■ REFERENCES

(1) Peeters, M.; Van Westen, G.; Li, Q.; IJzerman, A. *Trends Pharmacol. Sci.* **2011**, *32* (1), 35−42.

(2) White, A. D.; Keefe, A. J.; Ella-Menye, J.-R.; Nowinski, A. K.; Shao, Q.; Pfaendtner, J.; Jiang, S. *J. Phys. Chem. B* **2013**, *117* (24), 7254−7259.

(3) Hendsch, Z. S.; Tidor, B. *Protein Sci.* **1994**, *3* (2), 211−226.

(4) Pohl, P.; Saparov, S. M.; Pohl, E. E.; Evtodienko, V. Y.; Agapov, I. I.; Tonevitsky, A. G. *Biophys. J.* **1998**, *75* (6), 2868−2876.

(5) Cherepanov, D. A.; Feniouk, B. A.; Junge, W.; Mulkidjanian, A. Y. *Biophys. J.* **2003**, *85* (2), 1307−1316.

(6) Frauenfelder, H.; Petsko, G.; Tsernoglou, D. *Nature* **1979**, *280* (5723), 558−563.

(7) Zaccai, G. *Science* **2000**, *288* (5471), 1604−1607.

(8) Dong, M.; Husale, S.; Sahin, O. *Nat. Nanotechnol.* **2009**, *4* (8), 514−517.

(9) Rico, F.; Su, C.; Scheuring, S. *Nano Lett.* **2011**, *11* (9), 3983−3986.

(10) Medalsy, I.; Hensen, U.; Muller, D. J. *Angew. Chem., Int. Ed.* **2011**, *50* (50), 12103−12108.

(11) Dufrêne, Y. F.; Martínez-Martín, D.; Medalsy, I.; Alsteens, D.; Müller, D. J. *Nat. Methods* **2013**, *10* (9), 847−854.

(12) Stahlberg, H.; Fotiadis, D.; Scheuring, S.; Rémigy, H.; Braun, T.; Mitsuoka, K.; Fujiyoshi, Y.; Engel, A. *FEBS Lett.* **2001**, *504* (3), 166−172.

(13) Scheuring, S.; Müller, D. J.; Stahlberg, H.; Engel, H.-A.; Engel, A. *Eur. Biophys. J.* **2002**, *31* (3), 172−178.

(14) Ando, T.; Kodera, N.; Takai, E.; Maruyama, D.; Saito, K.; Toda, A. *Proc. Natl. Acad. Sci. U.S.A.* **2001**, *98* (22), 12468−12472.

(15) Kodera, N.; Yamamoto, D.; Ishikawa, R.; Ando, T. *Nature* **2010**, *468* (7320), 72−76.

(16) Uchihashi, T.; Iino, R.; Ando, T.; Noji, H. *Science* **2011**, *333* (6043), 755.

(17) Igarashi, K.; Uchihashi, T.; Koivula, A.; Wada, M.; Kimura, S.; Okamoto, T.; Penttilä, M.; Ando, T.; Samejima, M. *Science* **2011**, *333* (6047), 1279−1282.

(18) Preiner, J.; Kodera, N.; Tang, J.; Ebner, A.; Brameshuber, M.; Blaas, D.; Gelbmann, N.; Gruber, H. J.; Ando, T.; Hinterdorfer, P. *Nat. Commun.* **2014**, 5.

(19) Wang, Y.; Schulten, K.; Tajkhorshid, E. *Structure* **2005**, *13* (8), 1107−1118.

(20) Fu, D.; Libson, A.; Miercke, L. J.; Weitzman, C.; Nollert, P.; Krucinski, J.; Stroud, R. M. *Science* **2000**, *290* (5491), 481−486.

(21) Savage, D. F.; Egea, P. F.; Robles-Colmenares, Y.; O'Connell, J. D., III; Stroud, R. M. *PLoS Biol.* **2003**, *1* (3), e72.

(22) Hoomann, T.; Jahnke, N.; Horner, A.; Keller, S.; Pohl, P. *Proc. Natl. Acad. Sci. U.S.A.* **2013**, *110* (26), 10842−10847.

(23) Scheuring, S.; Ringler, P.; Borgnia, M.; Stahlberg, H.; Müller, D. J.; Agre, P.; Engel, A. *EMBO J.* **1999**, *18* (18), 4981−4987.

(24) Tseng, Q.; Duchemin-Pelletier, E.; Deshiere, A.; Balland, M.; Guillou, H.; Filhol, O.; Théry, M. *Proc. Natl. Acad. Sci. U.S.A.* **2012**, *109* (5), 1506−1511.

(25) Sbalzarini, I. F.; Koumoutsakos, P. *J. Struct. Biol.* **2005**, *151* (2), 182−195.

(26) Saparov, S. M.; Tsunoda, S. P.; Pohl, P. *Biol. Cell* **2005**, *97* (7), 545−550.

(27) Pohl, P.; Saparov, S. M.; Borgnia, M. J.; Agre, P. *Proc. Natl. Acad. Sci. U.S.A.* **2001**, *98* (17), 9624−9629.
(28) DeLano, W. L. 2002.

dx.doi.org/10.1021/nl504478f | *Nano Lett.* XXXX, XXX, XXX−XXX